

Measured and estimated wind speed of a stand-alone energy system with controlled bi-directional DC-DC battery bank

Ali Salam Al-Khayyat¹, Ahmed Kareem Abed¹, Amel Ahmed Ridha²

¹Department of Electrical and Electronics Engineering, Faculty of Engineering, University of Thi-Qar, Nasiriyah, Iraq

²Department of Electronics and Communication Engineering, Faculty of Engineering, University of Kufa, Kufa, Iraq

Article Info

Article history:

Received Sep 17, 2022

Revised Dec 16, 2022

Accepted Feb 15, 2023

Keywords:

Battery energy storage system
Estimated wind speed
Permanent magnet synchronous generator
Standalone wind turbine
STM32-based microcontroller

ABSTRACT

Simple control of a stand-alone variable speed wind turbine with a permanent magnet synchronous generator (PMSG) is presented in this paper. PMSG fed different types of loads by means of a converter where switched mode rectifier is connected to the PMSG, boost DC-DC converter, and voltage source inverter (VSI). The wind turbine is operated at measured wind speed and it is tested at estimated wind speed which is based on the power calculation of turbine power, generating electric power, losses power, and the dynamic power during the variation of wind speed. The estimation of wind speed would provide a scope of what a control method is applicable in practice and this would increase the performance by scheduling the connected loads. The bidirectional battery charger is controlled and used during the shortage of wind speed. The converter of the battery charger is controlled and implemented on an embedded system by using an STM32-based microcontroller. During the shortage or fluctuation of wind speed, the load voltage is controlled within the acceptable limit, where the voltage has been compensated. An extensive simulation has been conducted by MATLAB/Simulink, and the system shows a good dynamic response to the variation and decrease in wind speed.

This is an open access article under the [CC BY-SA](https://creativecommons.org/licenses/by-sa/4.0/) license.



Corresponding Author:

Ali Salam Al-Khayyat

Department of Electrical and Electronics Engineering, Faculty of Engineering, University of Thi-Qar
Nasiriyah, Iraq

Email: ali-al-khayyat@utq.edu.iq

1. INTRODUCTION

Due to the shortage of fossil fuels and environmental issues, the use of the conventional source of energy for power generation is considered the most difficult that most countries are facing. Wind energy is considered a non-conventional, clean, and infinite natural source of energy that is available to be used. The variable-speed wind turbine system has more advantages compared to the fixed speed in terms of output power maximization, mechanical stress reduction, efficiency increase, and quality power enhancement. Power electronic converters are crucial with the variable wind speed system, where at the generator side the AC is converted to DC and it is boosted to the desired value based on the requirement of the voltage source inverter (VSI), then it is converted to AC again with constant amplitude and frequency to feed the load. The reason for using permanent magnet synchronous generator (PMSG) over other types of generators is the reliability of the wind turbine system that operated at a variable speed, which could be improved with the use of PMSG. Simple structure, slow speed operation capability hence no need for a gearbox that would suffer from frequent faults and require maintenance. That leads to making the system unreliable, and self-excitation. A high power factor and operation with high efficiency are the advantages of using PMSG in variable-speed wind systems [1]–[3].

In the standalone system, the main challenge is to provide the customers with supply balanced voltage, and this would be performed by controlling an inverter, where in such systems, the energy is converted from DC to AC or AC to DC then to AC. The variations in the voltage are mainly caused due to the load changing. In the case of wind energy system, the fluctuations in wind speed would cause flickers which would reflect on the load voltage [3], [4]. Therefore, a stand-alone wind energy system is being developed. In [1]–[3], did not show how the bi-directional DC-DC converter would perform when there is no or shortage in wind speed. Bhende *et al.* [5] have not gone through the effect of load power and its variations. In [6], [7], did not show the response of battery bank and its control in the case of slow or absence of wind speed, and how it reacts to meet the power demand in this event. It's crucial to provide the load power needed in standalone wind energy systems, hence the battery energy storage system (BESS) is unavoidable. Since the change in the wind's speed causes to fluctuate the generated power from wind systems, the excess power is stored in an energy storage system, a battery. It is utilized to stabilize the supplied electricity to the load when the speed of the wind turbine is out of the speed limit. In addition, this BESS would also reduce the fluctuating power from the wind system and make the best use of power that is feeding the load, hence maximizing the reliability [8]–[13].

In this paper, simple control of a stand-alone variable speed wind turbine with a PMSG is proposed and investigated. The main contributions of this paper include: i) proposing a simple control for a stand-alone variable-speed wind energy system, and evaluating it in both measured and assessed wind conditions, ii) adjusting the PMSG switch mode rectifier to achieve sensorless maximum power point extraction from the available wind speed, iii) maintaining the system's power balance by keeping the DC-link voltage constant, where the bi-directional DC-DC converter is situated between the battery bank and the DC-link voltage, hence the important load can be fed in the event of a shortage or decrease in wind speed, and iv) additionally, the STM32-based microcontroller for generation pulse width modulation (PWM) of the bi-directional DC-DC converter is configured and used to implement the proposed proportional integral (PI) digital controller. The rest of the paper is organized into the following sections: in section 2, the variable speed of stand-alone wind energy system configuration is presented. Section 3 shows the mathematical modeling of the proposed system. The results and discussion are illustrated in section 4. Finally, the conclusion is presented in section 5.

2. VARIABLE SPEED STAND-ALONE WIND ENERGY SYSTEM CONFIGURATION

The system layout is shown in Figure 1. The system includes a wind turbine and a PMSG that is directly powered by the wind turbine. The PMSG is fed in single switch rectifier mode by a three-phase diode rectifier and a DC-DC boost converter, which supplies power to the VSI via a DC-link capacitor. At the DC-link capacitor, the bi-directional DC-DC battery charger is connected, where it supplies the VSI at the time when there is a shortage or drop in wind speed. The loads are connected to the VSI by LC filter [1]–[3], [5], [7], [8], [14]–[17].

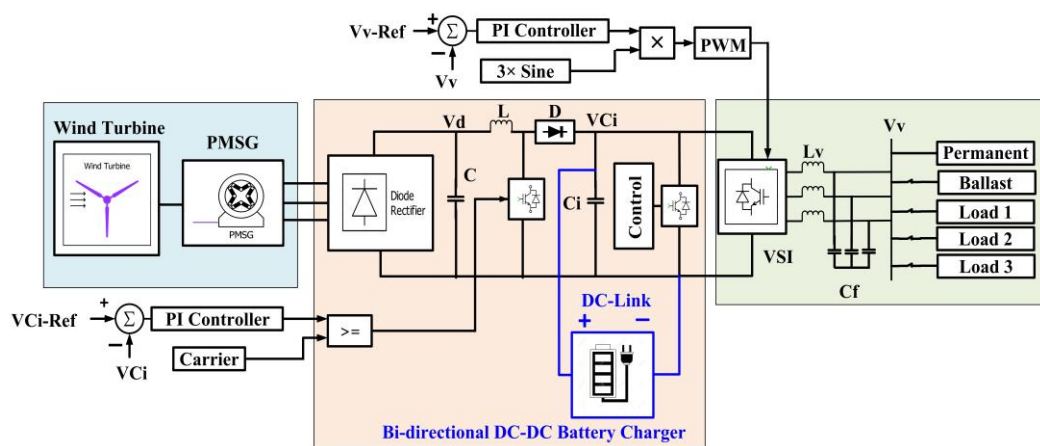


Figure 1. System diagram of the stand-alone wind energy system

3. SYSTEM MODELING

The system will be modeled and based on that it would be controlled. Firstly, the wind turbine would be modelled, then the DC-DC bi-directional battery bank is modelled and controlled after that the load

side inverter is controlled and finally, the wind speed is estimated based on the power calculations. The modeling is described as follows:

3.1. Wind turbine modeling

The wind turbine power (P_m) is expressed as (1):

$$P_m = 0.5 \rho A V_w^3 C_p(\lambda, \beta) = k_p V_w^3 C_p(\lambda, \beta) \tag{1}$$

Where ρ is the average air density and its value is 1.2 kg/m^3 , A is the rotor blade swept area of the turbine and it is given by πR^2 , where R is the length of the blade in meters. V_w is the speed of the wind in m/sec, C_p is the power coefficient and its value is determined by the tip speed ratio λ and the blade angle β . k_p is the proportionality factor and its value is $(0.5 \rho A)$. λ that is given by $\lambda = R \omega_r / V_w$, ω_r is the rotating speed of the rotor in rad/sec. It should be mentioned that usually ($2 < \lambda < 13$). C_p dependency on λ and each has a maximum value, therefore the rotation speed of the wind generator must vary with wind speed to maximize the power from the wind. Theoretically, the maximum value of C_p is 0.593. There are many expressions for $C_p(\lambda)$ based on the wind turbine design. In this paper the following expression is used [11], [13], [14], [18]–[23].

$$C_p(\lambda) = C_1 \left(\frac{C_2}{z} - C_3 \beta - C_4 \right) e^{-C_5/z} + C_6 \lambda \tag{2}$$

$$\frac{1}{z} = \frac{1}{\lambda + 0.08 \beta} - \frac{0.035}{1 + \beta^3} \tag{3}$$

Where $C_1 = 0.5176$, $C_2 = 116$, $C_3 = 0.4$, $C_4 = 5$, $C_5 = 21$ and $C_6 = 0.0068$ and they constants related to the wind turbine design and type. Based on these values, maximum C_p and λ are obtained and drawn as follows and it is found that $C_{pmax} = 0.48$ and $\lambda = 8.1$. it should be mentioned that the $C_p - \lambda$ curve is obtained for different values of β and it is shown in Figure 2.

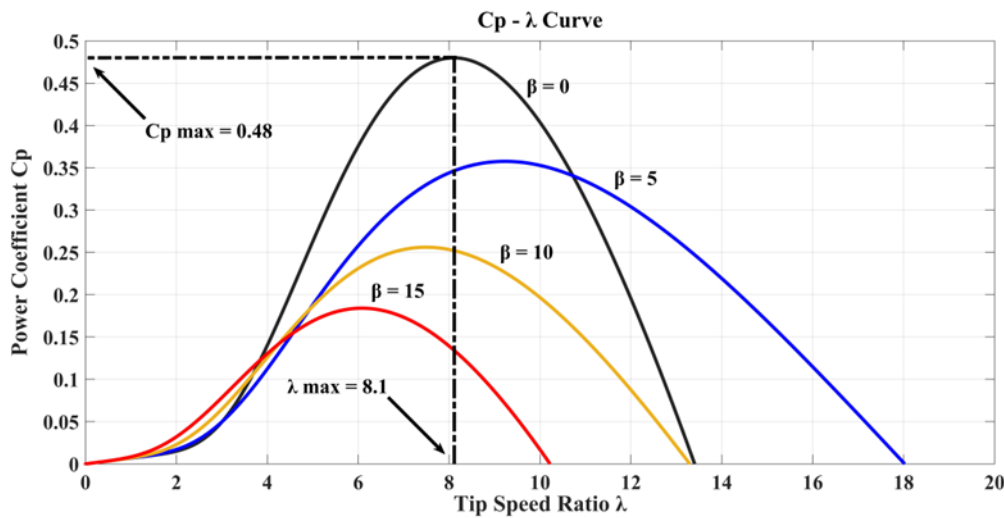


Figure 2. Dependent of power coefficient on tip speed ratio and rotor angle

The operation of the wind turbine at its optimum or maximum C_p results in the extraction of the most possible power from the wind turbine. Thus, it is essential to regulate the rotor speed at an optimum maximum tip speed ratio based on the available wind speed. The maximum output power from the wind turbine is expressed by (4) to (7).

$$P_{m-max} = (K_p C_{p-max} (R/\lambda_{max})^3) \omega_{r-opt}^3 \tag{4}$$

$$P_{m-max} = K_{p-opt} \omega_{r-opt}^3 \tag{5}$$

$$K_{p-opt} = (K_p C_{p-max} (R/\lambda_{max})^3) \quad (6)$$

$$\omega_{r-opt} = \frac{\lambda_{max}}{R} V_w \quad (7)$$

Where K_{p-opt} is the optimal proportionality factor, C_{p-max} is the maximum power coefficient and λ_{max} is the maximum tip speed ratio. Figure 3 shows the generated mechanical power by the wind turbine as a function of the rotational speed of the rotor for different values of wind speed. The maximum power from the wind could be extracted by controlling the converter at the generator side which is the switch mode rectifier.

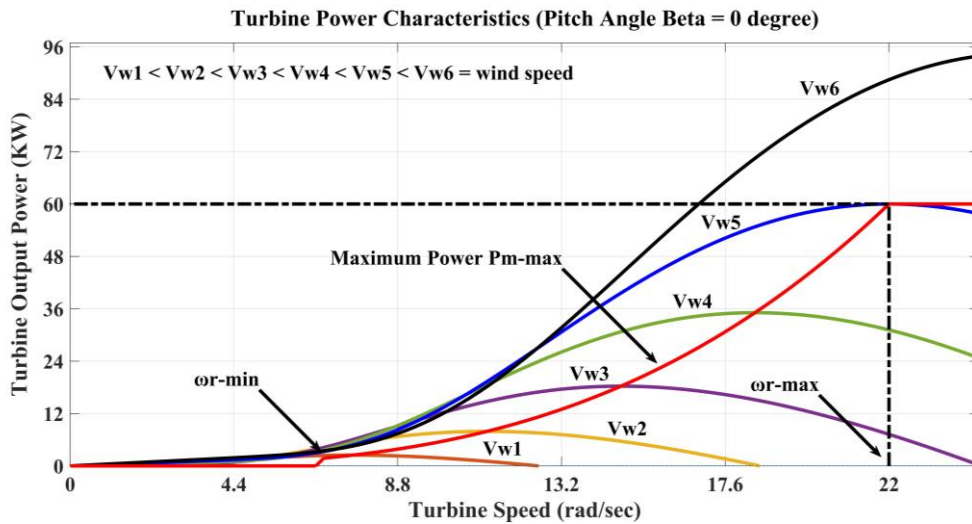


Figure 3. Turbine power characteristic with turbine output power versus turbine speed

The wind turbine's dynamic equation is given by the following equation, where it is directly connected to the PMSG:

$$J \frac{d\omega_m}{dt} = T_e - T_r - f\omega_m \quad (8)$$

Where J is the moment of inertia in Nm , T_r is the mechanical torque in Nm , T_e is the generator torque in $N-m$, and f is the viscous friction coefficient (kg/m^2). The main function of the rectifier is to change the generated AC voltage from the PMSG, which has a variable amplitude and frequency, into DC voltage. The maximum phase voltage (V_m) produced by the generator, which determines the value of the DC voltage and is given by (9):

$$V_{dc-rectifier} = \frac{3\sqrt{3}}{\pi} V_m \quad (9)$$

3.2. DC-DC boost converter modeling and control

The voltage of PMSG is rectified by the three-phase diode rectifier then it is boosted by the DC-DC boost converter. The main function of a boost converter is to change a fluctuating input DC voltage that results from various operating conditions into a suitable constant DC voltage. Controlling the converter duty cycle allows the DC-link voltage to be kept constant at the reference value, which is 500 V. The DC-DC boost converter's control structure is built on utilizing a PI-controller to keep the DC-Link voltage at the reference level as illustrated. The boost converter's input/output voltage and current relationships can be expressed mathematically. It needs to be mentioned that the switch of the DC-DC boost converter, which is usually insulated gate bipolar transistor (IGBT), is protected from blowing in case of over current. If the current passing through IGBT is exceeding 350 A, the IGBT is switched off and the gate pulse generation that follows would occur 0.1 s later when the current reaches 250 A [4], [6], [11], [24], [25].

$$V_{out} = \frac{1}{1-D} V_{in} \quad (10)$$

$$I_{dc-out} = (1 - D) I_{dc-in} \quad (11)$$

Where D is the duty cycle of the DC-DC boost converter.

3.3. DC-DC bi-directional battery charger modeling and control

For a stand-alone wind energy supply system, the battery storage system (BSS) is essential to maintain the balance between the generated power from wind turbines and the necessary power of the load throughout the process of charging or discharging energy to or from the energy storage system (ESS). The DC-DC buck-boost converter is used to connect the BSS to the DC link of the VSI. Controlling this system would keep the DC-link voltage V_{ci} shown in Figure 1, at a constant level, moreover, the control system would charge/discharge the current to/from the BSS based on the demand power from the load. The voltage of the battery is kept at a value less than the voltage of the DC-link, therefore the number of the batteries connected in series is less. In this paper, the output voltage of the DC-DC buck-boost converter is kept at 400 V and this system would provide the voltage to VSI in case of a drop or shortage of wind to supply the critical load. The state of charge (SOC) is 80% which is selected according to the assumption that even if there is a shortage in wind speed, the battery would be capable of providing power to the load of about 15 KW for about an hour. The battery rating is 61 Ahr [3], [6], [9]–[12], [15], [16], [19], [26]–[31].

The continuous conduction mode operation is used for the DC-DC bi-directional buck-boost converter as shown in Figure 4. The switches $Q1$ and $Q2$ are switched in a manner where the converter is operated with four sub-intervals in a steady state. The different steady-state operation cases of the converter are shown in Figure 5. In interval 1; the lower switch $Q2$ is turned on, while the upper switch $Q1$ is switched off when the diodes $D1$ and $D2$ are reverse biased, as shown in Figure 5(a). The inductor is charged and the current flowing through it increases during this time when the converter operates in boost mode. Interval 2; both switches $Q1$ and $Q2$ are off at this time. As seen in Figure 5(b), the diode $D1$ of the higher switch $Q1$ begins to conduct. In this interval, the converter powers the DC-link voltage. In interval 3; as depicted in Figure 5(c), the top switch $Q1$ is switched on and the bottom switch $Q2$ is turned off, while the diodes $D1$ and $D2$ are reversed bias. The converter switches to buck mode at this time and supplies the battery bank with energy. Interval 4; while both switches $Q1$ and $Q2$ are off during this time, the bottom switch's diode $D2$ begins to conduct, as seen in Figure 5(d).

The bi-directional DC-DC converter has two control loops; the outer loop regulates the DC-link voltage V_{ci} , while the inner loop regulates the battery current (I_b), as depicted in Figure 4. The bi-directional converter control charges and discharges the battery according to the battery SOC to maintain the V_{ci} . In terms of functionality, the switches $Q1$ and $S8$ complement one another. The IGBT $Q1$ and the IGBT $Q2$ anti-parallel diode, turn on while charging, making the converter run in buck mode. The converter works in boost mode as IGBT $Q2$ and the anti-parallel diode of IGBT $Q1$ becomes active while discharging. By feeding the V_{ci} error ($e_v = V_{ci-ref} - V_{ci}$) through a voltage PI controller, the desired battery current (I_b) is produced [9], [30]–[32]. Where Kp and KI are the proportional and integral gain of the PI controller.

$$I_{b-ref} = \left(Kp_v + \frac{KI_v}{s} \right) e_v \quad (12)$$

The required battery current (I_{b-ref}) is compared to the actual battery current (I_b), and the difference is used to create the modulation index (m) that controls the bi-directional DC-DC converter [33], [34]. It should be mentioned that low ripple current produced by the inductor on the battery bank side leads to improved efficiency and a long lifetime.

$$m = \left(Kp_i + \frac{KI_i}{s} \right) (I_{b-ref} - I_b) \quad (13)$$

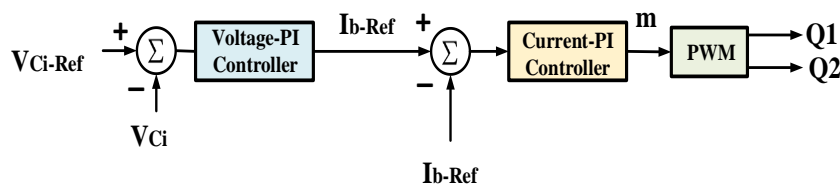


Figure 4. Bi-directional DC-DC control

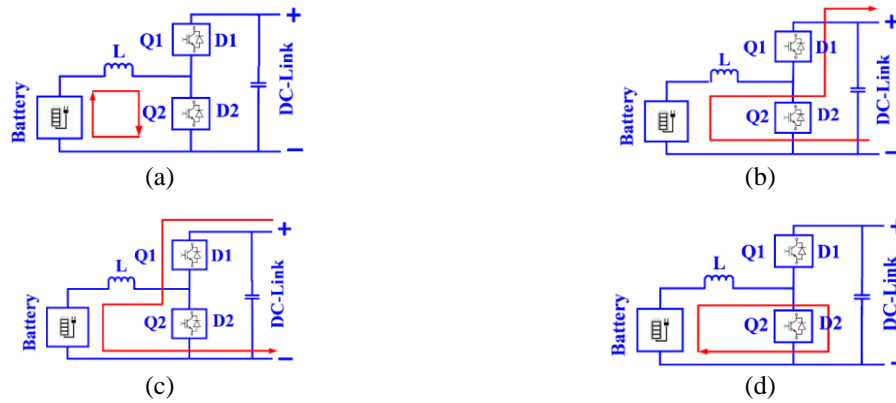


Figure 5. Bi-directional DC-DC battery charger operation circuit (a) interval 1, (b) interval 2, (c) interval 3, and (d) Interval 4

3.4. Modeling and control of load side converter

VSI is a converter located between the DC-link and load. The undesired high-frequency harmonics generated from the VSI are eliminated by placing the LC filter at the output of the VSI, this would improve the power quality at the load. There is no grid in the standalone wind energy system, therefore the function of the VSI is to regulate the frequency and voltage at the load side. The root mean square (RMS) value of the load line-to-line voltage is 220 V at 50 Hz frequency. The operation of the VSI is performed by PWM and there are two main techniques for this operation method, the first is the harmonic reference signal V_r is compared with triangle signal, which is usually known as carrier signal V_c and the second is space vector modulation SVM [5], [10], [20], [24], [25], [35], [36].

In the third-harmonic injection PWM, the three-phase reference signals V_{rabc} with amplitude m less than unity, $m \leq 1$ are controlled separately. For phase a , when the $V_{ra} < V_c$, the upper switch of the VSI leg A is switched-off when the logic is 0, and the lower switch is switched on and at this interval the potential of leg A is negative. The case is reversed when $V_{ra} > V_c$, where the potential is positive. Where V_{ra} is the reference voltage for phase a . The frequency of the carrier signal f_c is much higher than the frequency of the reference signal f_r , therefore the phase voltage average value with respect to the mid-point of period $1/f_c$ is V_{ra} [23]. The RMS value of fundamental line voltage is expressed in (14):

$$V_{phase-phase} = \frac{\sqrt{6}}{4} m V_{dc} = 0.612 m V_{dc} \tag{14}$$

Where V_{dc} is the voltage across the capacitor of the DC-link of the VSI. An adequate amplitude of zero sequence triple harmonics could be added to the three-phase reference signal, hence the linear operation region of PWM would be extended. The added amplitude signal (ΔV) is expressed as in (15). Therefore, the RMS value of fundamental line-to-line voltage is more by 1.15 compared the (14) as expressed in (16). The simple control diagram of VSI is shown in Figure 6.

$$\Delta V = -0.5[\max(V_{rabc}) + \min(V_{rabc})] \tag{15}$$

$$V_{phase-phase} = \frac{1}{\sqrt{2}} m V_{dc} = 0.707 m V_{dc} \tag{16}$$

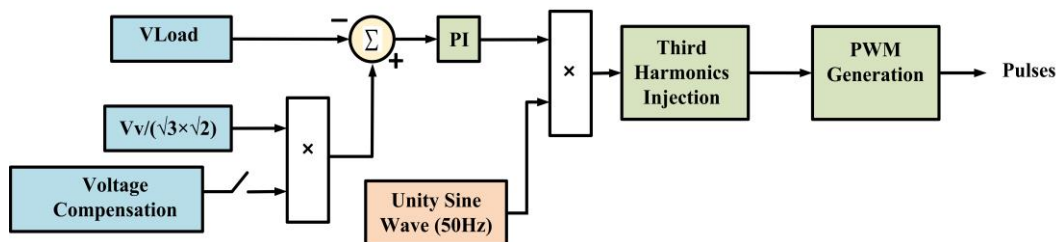


Figure 6. Load side VSI control diagram

3.5. Wind speed estimation modelling

Formula (1) states that the power of the turbine is dependent on the speed of the wind V_w and rotation speed of the rotor ω_r , therefore if the mechanical power of the turbine and rotor speed, the estimation wind speed would be obtained. An assumption is made, where the characteristic of the turbine is obtained by either calculation or experimental data. The turbine mechanical power P_m has not been measured, while the electrical power generated P_{el} could be calculated, then the estimated mechanical power P_{me} could be obtained as in (17):

$$P_{me} = P_{el} + P_{din} + P_{loss} \tag{17}$$

Where P_{loss} is the losses power which is the sum of core copper losses of generator winding, losses of ventilation, and friction losses and it is given as (18), and P_{din} is the dynamic power throughout the variation speed of rotation and is given as (19). Where I_s is the stator current of the PMSG, R_s is the stator resistor of the PMSG, F is the viscous friction coefficient and D is the ventilation coefficient and J is the total inertia. The block diagram of estimated wind speed is shown in Figure 7.

$$P_{loss} = I_s^2 R_s + (D + F \omega_r) \omega_r \tag{18}$$

$$P_{din} = J \omega \frac{d\omega}{dt} \tag{19}$$

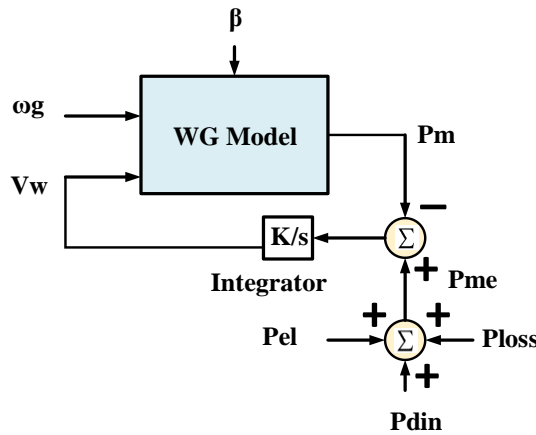


Figure 7. Block diagram of wind speed estimation

4. RESULTS AND DISCUSSION

MATLAB/Simulink is used to simulate the suggested control strategy for a standalone variable speed wind energy system under various operational conditions. The parameters used in the system are listed in Table 1. The load voltage is controlled at 220 V, and the RMS value and load phase voltage are shown in Figure 8(a) and (b) respectively.

Parameter	Value
Rated turbine output power P_m	60 kW
Rated rotational speed ω_r	22 rad/sec
DC-link voltage V_{ci}	500 V
Rated wind speed V_w	10 m/sec
Tip speed ratio λ	8.1
Power coefficient C_p	0.48
RMS load voltage V_v	220 V
Rated load frequency f_r	50 Hz
Bi-directional DC-DC output voltage	400 V

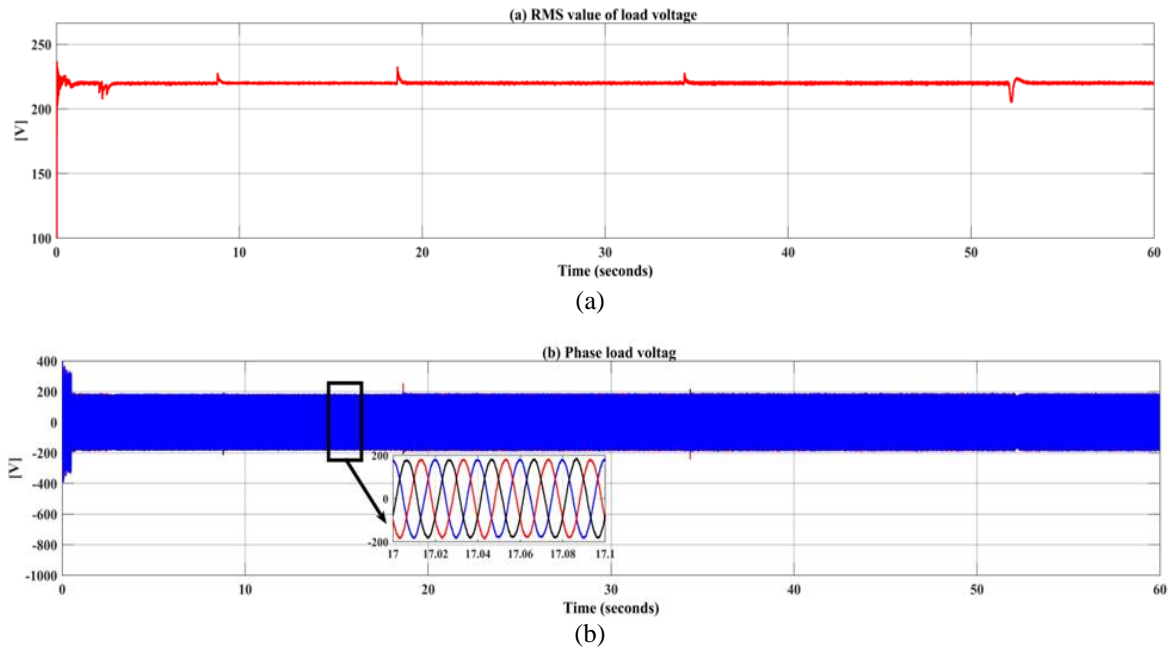


Figure 8. Load voltages, (a) RMS value of load voltage and (b) phase load voltage

The nominal power of the turbine in *p.u* is P_{m-nom} , the wind speed base V_{w-b} which is either wind speed mean value or predominant wind speed in the specific region, the *p.u* tip speed ratio is unity ($\lambda = \lambda_m$), ($C_p = C_{p-max}$), and the proportionality factor $K_p = 1$, therefore the (1) would be expressed as:

$$P_{m-nom-pu} = 1 \times \left(\frac{C_p}{C_{p-max}} \right) \times \left(\frac{V_w}{V_{w-base}} \right)^3 \quad (20)$$

$$P_{m-nom-pu} = \left(\frac{V_w}{V_{w-base}} \right)^3 \quad (21)$$

The load is made up of active-inductive components with the following powers: permanent load (10 kW) and switching on/off loads (13, 19, and 14 kW). The ballast load has a power output of (25.5 kW). From the turbine characteristic curve, it has been found that at the (22 rad/sec) rotating speed of wind generator, the ($P_e = 52.6$ kW) and that speed the turbine power is (60 kW). From that, the efficiency of the wind turbine is (87.7%). The required wind turbine power under ($P_e = 10 + 13 + 19 + 14 = 56$ kW) is (63.9 kW), which is ($63.9/60 = 1.065$ p.u). At the maximum power ($1.065 = (V_w/10)^3$), the wind speed is about (10.2 m/s). When the last load (14 kW) been switched off, then ($P_e = 56 - 14 = 42$ kW), and based on that the required wind turbine is (47.9 kW) that is about (0.8 p.u), and from that, the wind speed is (9.3 m/s). The load (19 kW) is switched off and ($P_e = 23$ kW) and the demanded wind turbine power is (26.6 kW) which is (0.437 p.u) and the wind speed for the operation with such load is (7.6 m/s). Under that condition where the wind turbine power is (0.19 p.u), the speed of the wind is (5.75 m/s) and at this wind speed the wind generator would stop and the load is fed from the battery bank that is feeding the VSI.

When the estimation wind speed method is employed, the selection of the load is constructed as follows; the same equation used for the modeling of wind turbine has been used for load selection. Under the same rotating speed, the powers P_1 at 8.8 m/s, P_2 at 9.8 m/s, and P_3 at 10.7 m/s are computed. Then these values of powers are compared with PMSG power P . The permanent load of 10 kW would remain if $P < P_1$. In addition to the permanent load, the load of 13 kW would be added if $P_1 < P < P_2$. The load of 19 kW is connected to the system if $P_2 < P < P_3$. The last load 14 kW is turned on when $P_3 < P$. After the system has been simulated it has figured out that the times of switching-off are 9, 17.8, and 34.2 s, which is the same as the actual wind speed. The response of measured and estimated wind speed is show in Figure 9(a), and the PMSG speed is illustrated in Figure 9(b) and it has observed that PMSG is stopped when the speed of the wind is (5.75 m/s). Turbine and load power responses are shown in Figure 9(c). Based on the selection of load, the drawn current would vary, the response of the current based on the selected load is shown in Figure 10. The total harmonic distortion (THD) of the phase load current is 1.92%.

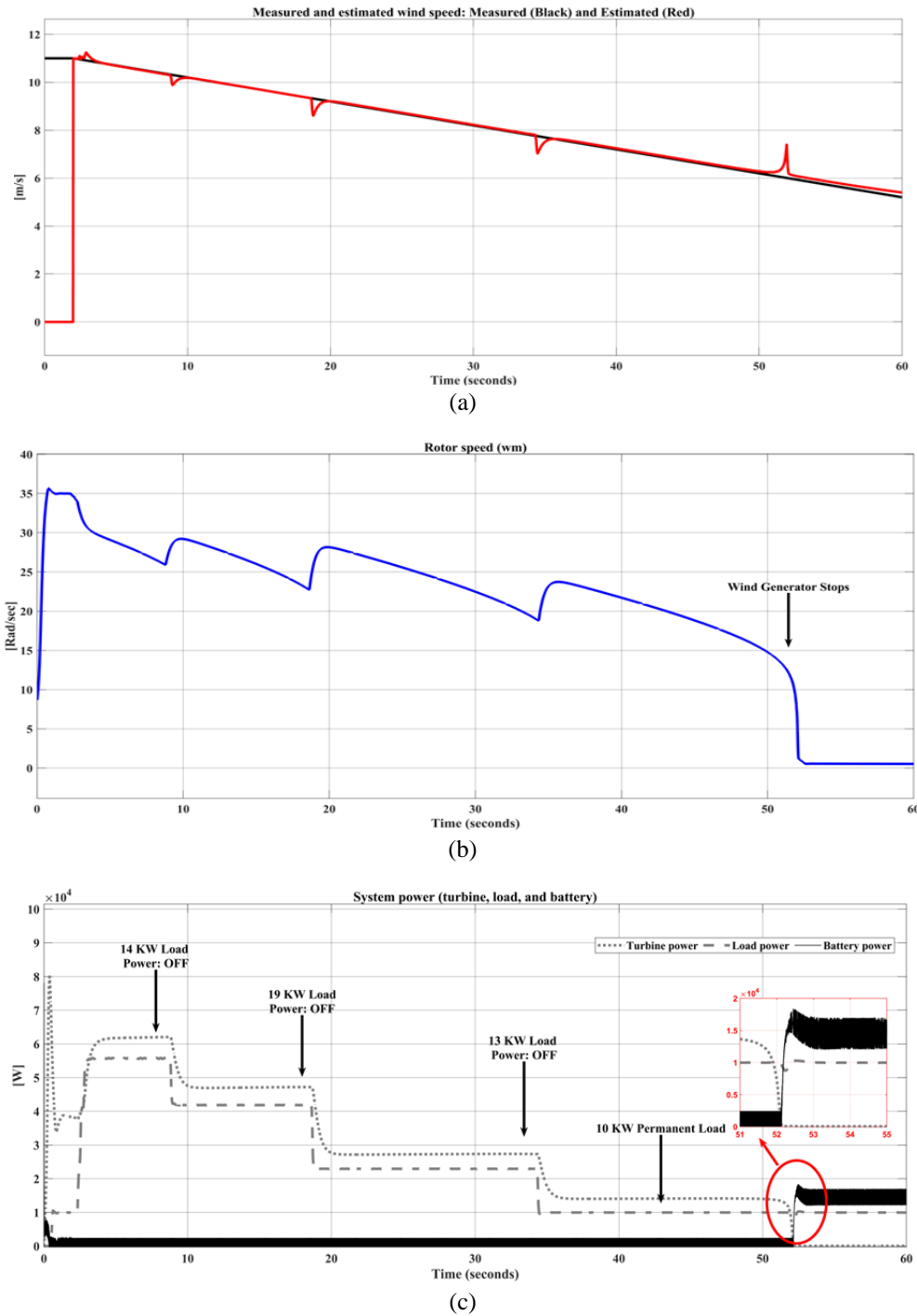


Figure 9. Responses of (a) measured and estimated wind speed, (b) PMSG speed, and (c) system power (turbine, load, and battery)

The maximum WG power at this wind speed is calculated in *p. u.* as $P_m = (V_w/10)^3$, and then this power is compared with the powers of the load sections while taking efficiency into consideration whether the system employs the wind speed V_w or its estimation V_{we} . When the WG power computed in this manner slightly exceeds the part power, the parts are switched off; when the calculated power levels are 5–10% higher than the switching-off values, the parts are switched on. The load voltage was maintained constant while the wind speed was estimated. With a deceleration of 0.1 m/s^2 , the wind speed is dropping starting at the instant $t = 2 \text{ s}$ from the original value of 11 m/s . After a short period, it can be seen that the amounts V_w and V_{we} are nearly equal until the WG ceases, at which point they are irrelevant. The load components are

turned off one by one at 8.8, 18.6, and 34.3 s. The wind speed is insufficient to supply the permanent load at $t = 52$ s. The battery now powers this load after the WG has stopped as shown in Figure 11(a), where the battery bank would feed the VSI. Figure 11(b) shows the SOC of the battery. The load voltage is precisely maintained. The response of DC-link voltage according to the wind speed is shown in Figure 11, where at $t = 52$ s and the VSI is fed from the battery bank to feed the permanent load.

The bi-directional DC-DC converter is controlled by digital PWM. The field programmable gate array (FPGA) is a powerful technology utilized by electronic system developers to implement hardware solutions without having to develop the elements of the electronic circuit. However, the cost of FPGA is high compared to microcontroller-based design. The choice of STM32-based microcontroller is based on compromising on three crucial factors: price, low power consumption, and performance. Hence a microcontroller STM32F3 with high speed (72 MHz) is utilized to implement the PWM controller, the PIN is shown in Figure 12. A bi-linear transformation is employed to represent the PI-based PWM part which is shown in Figure 4. The code of the program is written in C language under the Keil environment. Figure 12 shows the pin connection of STM32F3. In the configuration stage, PA1 and PA2 were configured as high-speed output general-purpose input/output (GPIO) for boosting and bucking mode signals. In order to read the measured voltage by the microcontroller, an ADC1 was configured to read the input voltage on pin PA12 and attenuated to be appropriate for microcontroller's voltage levels. A general-purpose timer TIM3 is configured and driven by 1 MHz to obtain a delay function with 1 microsecond which is used to generate precise PWM signals (output 1 & output 2) where the generated duty cycle D is restricted by a range: $1\mu sec \leq D \leq 10\mu sec$. Figure 13(a) illustrates the output of the two control signals in both modes: the boosting and the bucking mode, which is identical to the pulses in Figure 13(b) which is the result from system simulation.

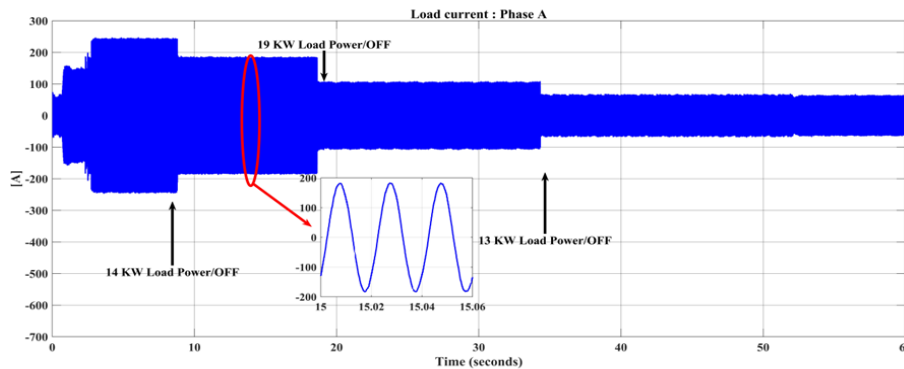
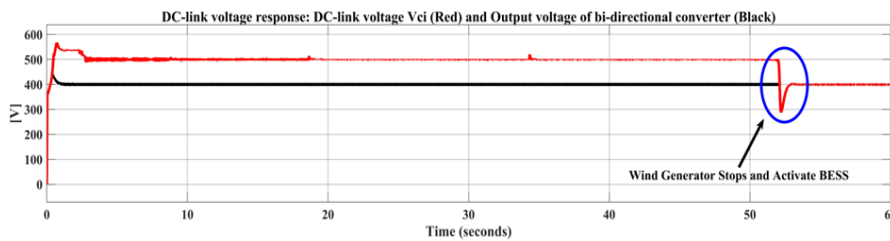
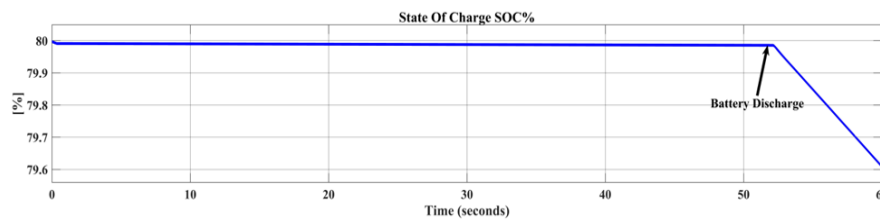


Figure 10. The load current of phase A



(a)



(b)

Figure 11. DC-link voltage and output voltage of bi-directional battery charger (a) DC link voltage response and (b) SOC of the battery bank

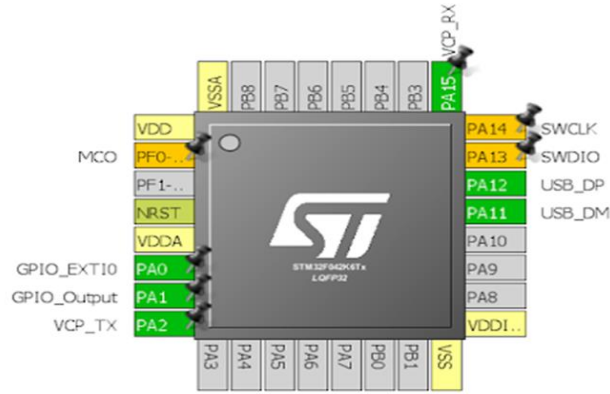


Figure 12. The STM32F303 pins connection for generating PWM signals

In order to increase the time between the certain part which is switched on and the speed of the wind. If this part is switched off, it is reasonable to lower the load voltage while still operating within the limits of the current standards by reducing V_w . The result of this measurement depends on how much the power loads vary on the provided voltage. When a certain load component is turned on and off, it is possible to reduce the load voltage within acceptable limits by allowing V_w to drop in order to widen the gap between the wind speeds. The load voltage is adjusted to 220 V when a specific load part is turned on; with the wind speed lowers, the voltage drops by 10%. The response of the RMS value of load voltage as a function of decreasing wind speed is shown in Figure 14, where the load parts turning off times are $t = 9, 19,$ and 40 sec.

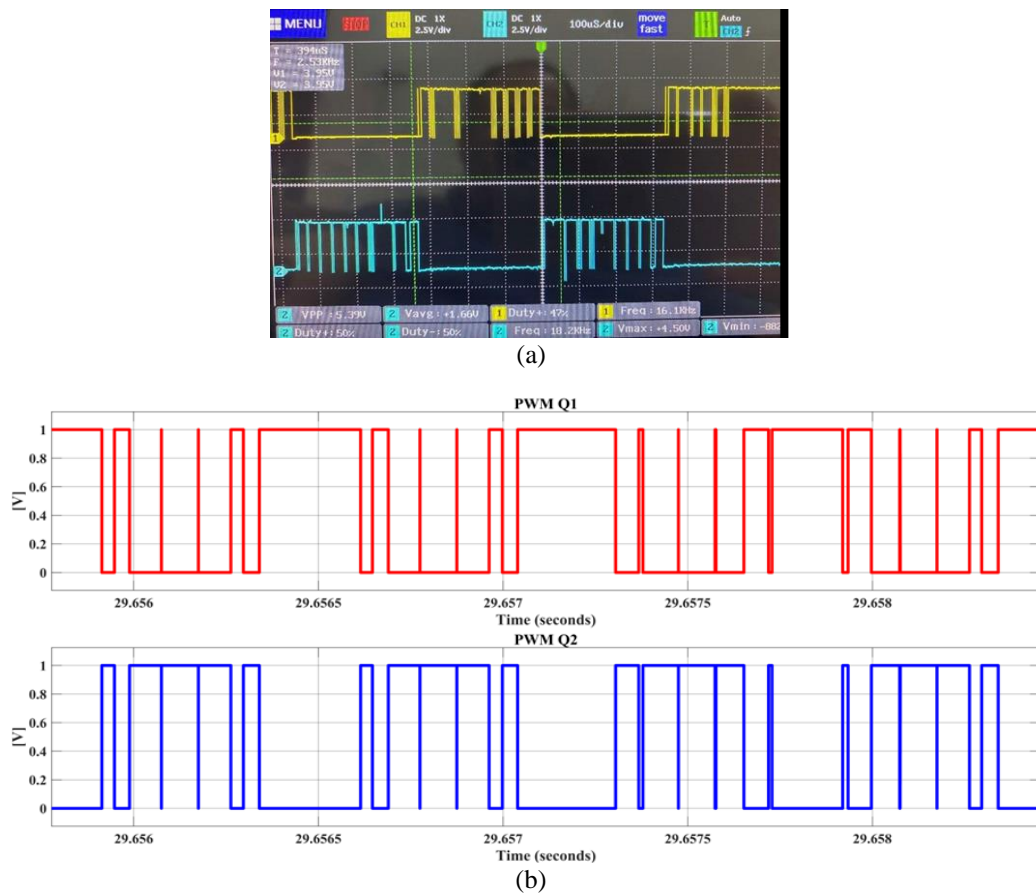


Figure 13. The PWM signals for buck-boost mode (a) experimental and (b) simulation

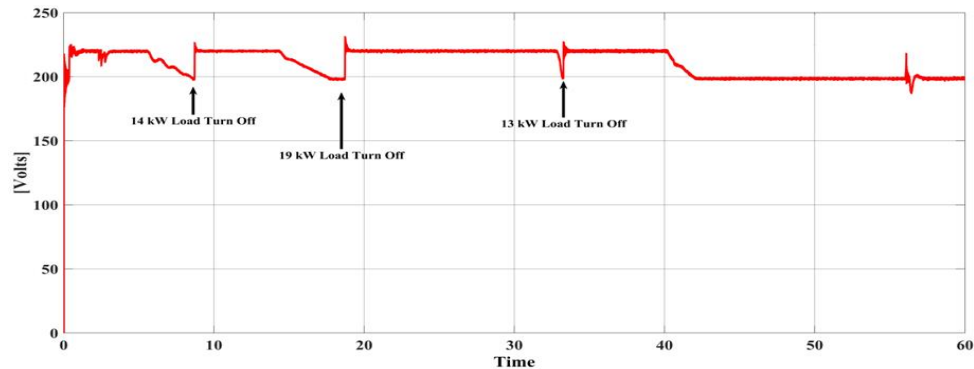


Figure 14. RMS value of load voltage at decreasing wind speed

5. CONCLUSION

Simple control of a variable speed stand-alone wind energy system has been presented and each part of the system has been analyzed and modeled. The system has been simulated and tested under measured and estimated wind speed and the results are compared. The voltage from PMSG has been controlled and boosted by the DC-DC boost converter which fed the VSI, moreover, by managing the DC-DC bidirectional buck-boost converter, which is coupled to the battery bank and the DC-link voltage, the battery bank has been able to store the excess wind energy and supply it to the load during a wind power shortage. Due to its fast response and cost-effectiveness, the STM32-based microcontroller is used for generating two PWM signals to control IGBT switches of the bi-directional DC-DC converter. The load voltage is controlled and compensated during the variation in the wind speed, and the power loads. The simulation results demonstrated that despite variations in wind speed and loads, the control technique has a good dynamic response.

ACKNOWLEDGEMENTS

The authors would like to thank the Department of Electrical and Electronics Engineering at University of Thi-Qar for sponsoring this research.




REFERENCES

- [1] M. Hussein, T. Senjyu, M. Orabi, M. Wahab, and M. Hamada, "Control of a stand-alone variable speed wind energy supply system," *Applied Sciences*, vol. 3, no. 2, pp. 437–456, 2013, doi: 10.3390/app3020437.
- [2] A. S. Satpathy, N. K. Kishore, D. Kastha, and N. C. Sahoo, "Control scheme for a stand-alone wind energy conversion system," *IEEE Transactions on Energy Conversion*, vol. 29, no. 2, pp. 418–425, 2014, doi: 10.1109/TEC.2014.2303203.
- [3] M. D. Vijay, B. Singh, and G. Bhuvaneshwari, "Standalone and grid connected operations of a SynRG based WECS with BESS," in *2018 IEEMA Engineer Infinite Conference (eTechNxt)*, 2018, pp. 1–6, doi: 10.1109/ETECHNXT.2018.8385286.
- [4] L. Stefan and F. Yusivar, "Modeling of wind turbine generator with boost converter MPPT," in *2018 2nd International Conference on Smart Grid and Smart Cities (ICSGSC)*, 2018, pp. 100–104, doi: 10.1109/ICSGSC.2018.8541306.
- [5] C. N. Bhende, S. Mishra, and S. G. Malla, "Permanent magnet synchronous generator-based standalone wind energy supply system," *IEEE Transactions on Sustainable Energy*, vol. 2, no. 4, pp. 361–373, 2011, doi: 10.1109/TSTE.2011.2159253.
- [6] J.-H. Lee, D.-Y. Jung, T.-K. Lee, Y.-R. Kim, and C.-Y. Won, "Regenerative current control method of bidirectional DC/DC converter for EV/HEV application," *Journal of Electrical Engineering and Technology*, vol. 8, no. 1, pp. 97–105, 2013, doi: 10.5370/JEET.2013.8.1.097.
- [7] M. Druga, C. Nichita, G. Barakat, and E. Ceanga, "Stand-alone wind power system operating with a specific storage structure," *Renewable Energy and Power Quality Journal*, vol. 1, no. 7, pp. 291–296, 2009, doi: 10.24084/repqj07.332.
- [8] B. Singh and S. Sharma, "Stand-alone wind energy conversion system with an asynchronous generator," *Journal of Power Electronics*, vol. 10, no. 5, pp. 538–547, 2010, doi: 10.6113/JPE.2010.10.5.538.
- [9] H. F. Khazaal, I. S. Hburi, M. S. Farhan, and M. Dininawi, "A hybrid control strategy for PMSG-based standalone wind turbines with BESS," *IOP Conference Series: Materials Science and Engineering*, vol. 745, no. 1, pp. 1–13, 2020, doi: 10.1088/1757-899X/745/1/012012.
- [10] D. Cloete and S. Chowdhury, "Load controller for a stand alone variable speed wind energy conversion system with energy storage," in *2021 IEEE PES/IAS PowerAfrica*, 2021, pp. 1–5, doi: 10.1109/PowerAfrica52236.2021.9543145.
- [11] H. Ahmed and A. Bhattacharya, "PMSG based constant power delivery standalone WECS using SST with bidirectional buck-boost BESS," in *2016 IEEE 7th Power India International Conference (PIICON)*, 2016, pp. 1–6, doi: 10.1109/POWERI.2016.8077238.
- [12] A. Rajaei, S. Yazdani, and E. Ebadi, "PMSG-based stand-alone wind energy conversion system using quasi Y-source inverter and battery storage," in *2022 13th Power Electronics, Drive Systems, and Technologies Conference (PEDSTC)*, 2022, pp. 81–85, doi: 10.1109/PEDSTC53976.2022.9767305.
- [13] S. R. Mhandu and O. M. Longe, "Techno-economic analysis of hybrid PV-wind-diesel-battery standalone and grid-connected microgrid for rural electrification in Zimbabwe," in *2022 IEEE Nigeria 4th International Conference on Disruptive Technologies*




- for Sustainable Development (NIGERCON), 2022, pp. 1–5, doi: 10.1109/NIGERCON54645.2022.9803058.
- [14] M. López and J.-C. Vannier, “Stand-alone wind energy conversion system with maximum power transfer control,” *Ingeniare. Revista chilena de ingeniería*, vol. 17, no. 3, pp. 329–336, 2009, doi: 10.4067/S0718-33052009000300006.
- [15] T.-L. Pan, H.-S. Wan, and Z.-C. Ji, “Stand-alone wind power system with battery/supercapacitor hybrid energy storage,” *International Journal of Sustainable Engineering*, vol. 7, no. 2, pp. 103–110, 2014, doi: 10.1080/19397038.2013.779327.
- [16] Z. F. Khan and R. Gupta, “Standalone wind energy conversion system for EV battery charging and AC residential loads,” in *IECON 2021–47th Annual Conference of the IEEE Industrial Electronics Society*, 2021, pp. 1–6, doi: 10.1109/IECON48115.2021.9589115.
- [17] H. A. Rabab’ah and Y. N. Anagreh, “Modeling and simulation of standalone WECS-PMSG for water pumping system,” in *2021 IEEE PES/IAS PowerAfrica*, 2021, pp. 1–5, doi: 10.1109/PowerAfrica52236.2021.9543189.
- [18] M. Najafi, M. Siah, R. Ebrahimi, and M. Hoseynpoor, “A new method to control of variable speed wind generation system connected to permanent magnet synchronous generator,” *Australian Journal of Basic and Applied Sciences*, vol. 5, no. 5, pp. 433–440, 2011.
- [19] R. Patel, K. Arora, and S. Katiyar, “Control analysis of PMSG based wind energy conversion system using buck-boost converter,” in *2016 Second International Conference on Computational Intelligence & Communication Technology (CICT)*, 2016, pp. 395–402, doi: 10.1109/CICT.2016.84.
- [20] F. Z. Naama, A. Zegaoui, Y. Benyssaad, F. Z. Kessaissia, A. Djahbar, and M. Aillerie, “Model and simulation of a wind turbine and its associated permanent magnet synchronous generator,” *Energy Procedia*, vol. 157, pp. 737–745, 2019, doi: 10.1016/j.egypro.2018.11.239.
- [21] G. Mehta, “Modelling and simulation of wind turbine generator in MATLAB/Simulink,” *International Journal for Research in Applied Science and Engineering Technology*, vol. 8, no. 6, pp. 849–852, 2020, doi: 10.22214/ijraset.2020.6137.
- [22] F. Echiheb *et al.*, “Robust sliding-backstepping mode control of a wind system based on the DFIG generator,” *Scientific Reports*, vol. 12, no. 1, pp. 1–16, 2022, doi: 10.1038/s41598-022-15960-7.
- [23] M. F. Elmorshedy, S. M. Allam, A. I. A. Shobair, and E. M. Rashad, “Voltage and frequency control of a stand-alone wind-energy conversion system based on PMSG,” in *2015 4th International Conference on Electric Power and Energy Conversion Systems (EPECS)*, 2015, pp. 1–6, doi: 10.1109/EPECS.2015.7368494.
- [24] P. Kashyap and P. Mahalingam, “Non-isolated high step-up DC-DC converter with low input current ripple,” in *2021 IEEE International Power and Renewable Energy Conference (IPRECON)*, 2021, pp. 1–6, doi: 10.1109/IPRECON52453.2021.9640764.
- [25] F. Asghar, M. Talha, and S. Kim, “Robust frequency and voltage stability control strategy for standalone AC/DC hybrid microgrid,” *Energies*, vol. 10, no. 6, pp. 1–20, 2017, doi: 10.3390/en10060760.
- [26] J.-H. Kuo, W.-Y. Wang, and K.-Y. Lo, “Step-up battery charger for stand-alone wind power system,” in *2019 IEEE 4th International Future Energy Electronics Conference (IFEEEC)*, 2019, pp. 1–5, doi: 10.1109/IFEEEC47410.2019.9014975.
- [27] P. Sahin, R. Resmi, and V. Vanitha, “PMSG based standalone wind electric conversion system with MPPT,” in *2016 International Conference on Emerging Technological Trends (ICETT)*, 2016, pp. 1–5, doi: 10.1109/ICETT.2016.7873701.
- [28] N. Mararakanye and S. Chowdhury, “DC-link based control system for a stand-alone variable speed wind energy conversion system with storage,” in *25th Southern African Universities Power Engineering Conference*, 2017, pp. 760–765.
- [29] S. Susanna, B. R. Dewangga, O. Wahyungoro, and A. I. Cahyadi, “Comparison of simple battery model and thevenin battery model for SOC estimation based on OCV method,” in *2019 International Conference on Information and Communications Technology (ICOIACT)*, 2019, pp. 738–743, doi: 10.1109/ICOIACT46704.2019.8938495.
- [30] K. M. Tan, V. K. Ramachandaramurthy, and J. Y. Yong, “Bidirectional battery charger for electric vehicle,” in *2014 IEEE Innovative Smart Grid Technologies-Asia (ISGT ASIA)*, 2014, pp. 406–411, doi: 10.1109/ISGT-Asia.2014.6873826.
- [31] M.-Y. Ke, Y.-H. Chiu, and C.-Y. Wu, “Battery modelling and SOC estimation of a LiFePO4 battery,” in *2016 International Symposium on Computer, Consumer and Control (IS3C)*, 2016, pp. 208–211, doi: 10.1109/IS3C.2016.63.
- [32] H. N. d. Melo, J. P. F. Trovao, P. G. Pereirinha, H. M. Jorge, and C. H. Antunes, “A controllable bidirectional battery charger for electric vehicles with vehicle-to-grid capability,” *IEEE Transactions on Vehicular Technology*, vol. 67, no. 1, pp. 114–123, 2018, doi: 10.1109/TVT.2017.2774189.
- [33] M. E. Haque, K. M. Muttaqi, and M. Negnevitsky, “Control of a stand alone variable speed wind turbine with a permanent magnet synchronous generator,” in *2008 IEEE Power and Energy Society General Meeting-Conversion and Delivery of Electrical Energy in the 21st Century*, 2008, pp. 1–9, doi: 10.1109/PES.2008.4596245.
- [34] M. B. Hariz, F. Bouani, and M. Ksouri, “Implementation of a fixed low order controller on STM32 microcontroller,” in *International Conference on Control, Engineering & Information Technology (CEIT’14)*, 2014, pp. 244–252.
- [35] P. Anbarasan, M. Venmathi, and V. Krishnakumar, “Modeling and simulation of standalone PMSG based wind energy conversion system with common mode voltage suppression,” in *2021 7th International Conference on Electrical Energy Systems (ICEES)*, 2021, pp. 85–88, doi: 10.1109/ICEES51510.2021.9383728.
- [36] N. Güler, E. Irmak, H. Gör, and E. Kurt, “An inverter design for a new permanent magnet synchronous generator,” *International Journal of Hydrogen Energy*, vol. 42, no. 28, pp. 17723–17732, 2017, doi: 10.1016/j.ijhydene.2017.01.223.

BIOGRAPHIES OF AUTHORS






Ali Salam Al-Khayyat    received the B.Sc. degree in Electrical Engineering from University of Kufa, Iraq in 2008, and the M.Sc. degree in Electrical Engineering for Sustainable and Renewable Energy System from University of Nottingham, UK in 2014. He joined the faculty of Engineering in University of Thi-Qar since 2016. He is currently lecturer at the Department of Electrical and Electronics Engineering in University of Thi-Qar. His research interests are power electronic control, power quality, and renewable energy. He can be contacted at email: ali-al-khayyat@utq.edu.iq.



Ahmed Kareem Abed    was born in Nasiriya city, Iraq in January 1975. He received the B.Sc. degree in Electrical Engineering and M.Sc. degree in Electrical and Communication Engineering from the University of Basra, Mustansiriyah University (Baghdad), Iraq, in 1996 and 1999, respectively. Between 1998 and 1999, he worked a scientific researcher at the Iraqi Space Research Center, Baghdad, Iraq. Since then, in 2005, he joined the Department of Electrical and Electronics Engineering, University of Thi-Qar (Iraq), as a lecturer where he taught many subjects in electric, control, computer, and communication systems. He is an IEEE member since 2016. He participated with four IEEE conference papers in US. In 2019, he received the Ph.D. degree from the Department of Electronic and Computer Engineering, College of Engineering and Applied Science, Western Michigan University, Michigan, USA. Also, he was appointed as a research scientist at AhuraTech LLC, Michigan, USA from 2020 to 2021. His Ph.D topic is WLAN-based indoor positioning systems. In addition, he is interested with other subjects such as sensor networks, machine learning, embedded systems-based design, and digital signal processing for communication. He published more than 20 journals and papers in these scientific areas. He can be contacted at email: ahmed.abed@utq.edu.iq.



Amel Ahmed Ridha    is a lecturer in Electronic and Communications Engineering Department, University of Kufa, Iraq since 2011; and she has been a senior lecturer since 2005. She received the B.Eng. degree in electrical engineering, the M.Eng. and Ph.D. degree in Electrical Power Engineering from University of Technology, Baghdad, Iraq in 1991, 1998 and 2005, respectively. She had completed training course in Cardiff University in 2014. Her research interests include the field of power electronics, motor drives, industrial applications, industrial electronics, photovoltaic power systems, and field programmable logic control applications. She can be contacted at email: amala.alsudani@uokufa.edu.iq.